Organic Process Research & Development **2008,** *12,* 837–849

Particle Shape Characterisation via Image Analysis: from Laboratory Studies to In-process Measurements Using an in Situ Particle Viewer System

Rui Fa Li, Radoslav Penchev, Vasuki Ramachandran, Kevin J. Roberts,* and Xue Z. Wang

Institute of Particle Science and Engineering, School of Process, Environmental and Materials Engineering, University of Leeds, Leeds LS2 9JT, U.K.

Richard J. Tweedie, and Andy Prior

Malvern Instruments Ltd., Enigma Business Park, Malvern, Worcestershire WR14 1XZ, U.K.

Jan W. Gerritsen, and Fred M. Hugen

Perdix Analytical Systems B.V., Everarduspstein 6, 6602 EP Wijchen, The Netherlands

Abstract:

A recent evaluation of a new in situ particle viewer (ISPV) system for the examination of particle shape and its subsequent development during crystal growth is presented. Precharacterization studies using conventional and hot-stage microscopy reveal that the ISPV probe system together with a commercial image analysis software is capable of generating representative high-quality images which can be processed and analysed. ISPV studies of the batch crystallization of L-glutamic acid in a 20-L reactor are shown to be able to characterise effectively crystallization and polymorphic phase transformation processes, revealing potential applications in both small- and large-scale reactor systems. Some improvements to the probe, such as increasing the resolution and reducing the encrustation using thermal coating, are suggested.

1. Introduction

Crystallization from solution is an important unit operation for the isolation and subsequent separation of many speciality pharmaceutical compounds. It confers the additional advantage of enhancing product purity, thus reflecting the molecular recognition of solute to solute inherent in the self-assembly process underpinning crystallization. Increasing economic pressure to reduce process development costs whilst improving product quality has led to a significant amount of research in the crystallization area in order to improve process understanding. An important component in such developments involves the development of Process Analytical Technology[1] (PAT) through which manufacturing processes can, in principle, be monitored against benchmarks and subsequently controlled and optimised to produce high-quality products in the desired solid physical form (morphology and through its analysis, polymorphic form). Important physical quality-related parameters of significant industrial application relate to crystal size and its associated shape. This is important for many materials reflecting the impact of particle size and shape on, e.g., product purity[3,4,5] (and vice versa), downstream processing (filtration, dissolution rate, tableting), and product formulation. The effective measurement and control of crystal size is hence important in improving product quality of the crystals produced in the batch crystallization and polymorphic transformation processes. In a manner similar to that of crystal size, morphology of crystals plays an important role, and crystal shape can influence various processes including blending, milling, and drying.

This perspective forms the basis of this paper which reviews some recent trial studies of the use of in-process crystal size measurement using a combination of laboratory microscopy precharacterisation together with the application of an in situ particle viewer (ISPV) developed by PERDIX Technologies B.V., Netherlands, at the 20-L scale size associated with the batch crystallization of the amino acid L-glutamic acid (L-GA). L-GA forms a useful representative compound for understanding the crystallization of speciality and pharmaceutical compound. This paper also provides brief overviews on in-process technique for assessing crystal size/shape and on the crystallization and phase transformation of L-GA.

2. Techniques for In Situ Particle Size and Shape Characteristics

A brief overview of in-process techniques for measuring crystal size distribution (CSD) are available.[6,7] Laser light-scattering techniques are popular methods for particle charac-

* Corresponding author: E-mail: K.J.Roberts@leeds.ac.uk.

(1) Shekunov, B. Y.; Chattopadhyay, P.; Tong, H. H. Y.; Chow, A. H. L. *Pharm. Res.* **2007**, *24*, 203.
(2) Yu, L. X.; Lionberger, R. A.; Raw, A. S.; D'Costa, R.; Wu, H.; Hussain, A. S. *Adv. Drug Delivery Rev.* **2004**, *56*, 349.
(3) Walker, E. M.; Roberts, K. J.; Maginn, S. J. *Langmuir* **1998**, *14*, 5620.
(4) Stocia, C.; Verwer, P.; van Hoof, P.J.C.M.; Kaspersen, F. M.; Vlieg, E. *Crystal Growth Des.* **2004**, *4*, 765.
(5) Clydesdale, G.; Roberts, K. J.; Telfer, G. B.; Grant, D. J. W. *J. Pharm. Sci.* **1997**, *86*, 135.
(6) Allen, T. *Particle Size Measurement*; Chapman & Hall: London, 1974, 1997.
(7) Provder, T., Texter, J., Eds. *Particles Sizing and Characterization*; American Chemical Society: Washington DC, 2004.
(8) Barth, H. G. *Modern Methods of Particle Size Analysis*; John Wiley & Sons: NJ, 1984.

10.1021/op800011v CCC: $40.75
Published on Web 07/30/2008

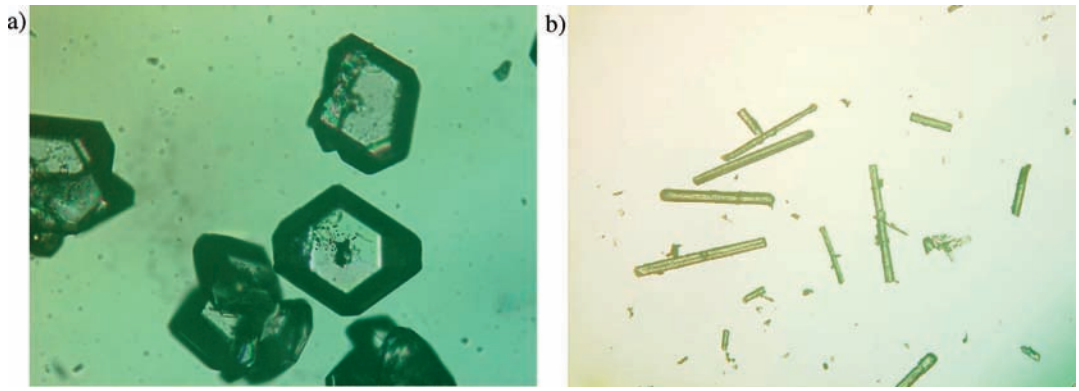

Figure 1. **Microscope images of crystals of L-glutamic acid: (a) the platelike α-form; (b) needlelike *β*-form.**

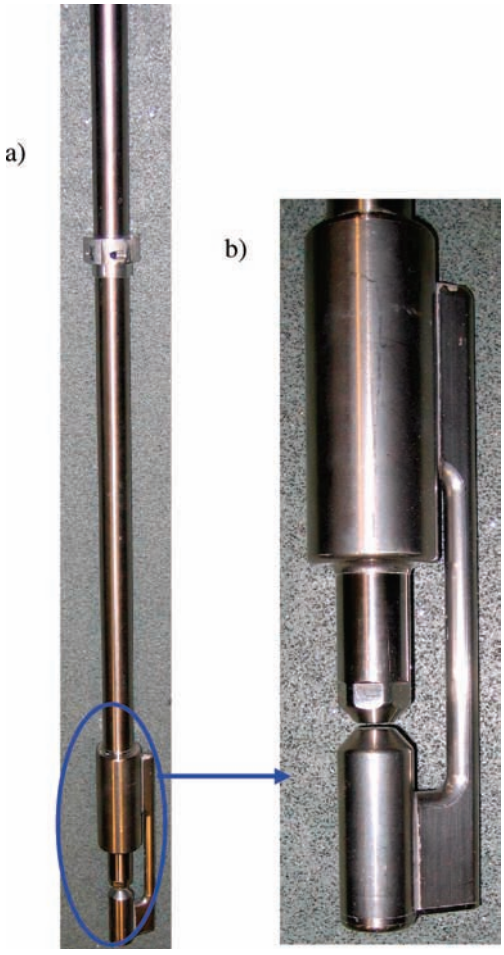

Figure 2. **(a) In situ particle viewer (ISPV) probe (dimensions 50 mm × 30 mm × 120 mm), (b) enlargement of the system's sensor-head.**

terisation and are based on the inverse relationship of the angle of the scattered light by particles to the particle size. In this, a beam of monochromatic light interacts with the particles which scatter the light at various angles.[9] Large particles scatter light at narrow angles with high intensity, whereas small particles scatter light at wide angles but with low intensity, thus forming a diffraction pattern. The diffraction pattern can be analysed using Mie theory to give a realistic estimation of the size. For

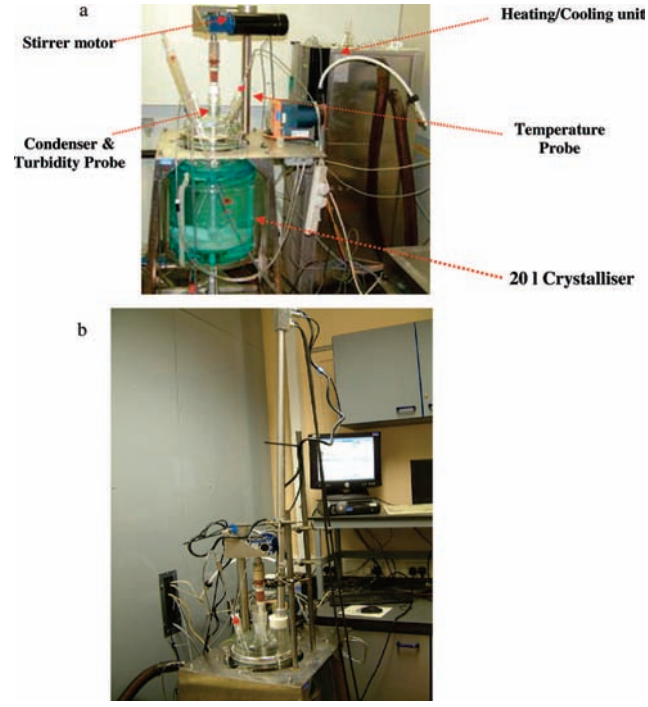

Figure 3. **HEL Autolab batch reactor (20 L) set up with the ISPV probe system: (a) reactor and (b) probe inserted into part of a reactor head.**

example, the Mastersizer 2000[10] system uses laser light scattering and Mie theory to solve the equations for interaction of light with particles. With particles in the size range, usually defined as volume (V), the equivalent diameter (D) of a sphere ($V = \pi/6D^3$) between 0.02 and 2000 μm can be measured with this instrument. A significant limitation of this technique is that the samples for measurement have to be diluted if their solid fraction concentration is above 0.1 vol % of solids. Whilst crystal shape information can also in principle be derived using laser diffraction techniques, i.e. using the azimuthal light intensity distribution as reported by Scarlett et al.,[11] such approaches are not routine, and commercial instruments for this are not currently available.

Back-scattering approaches provide an alternative to traditional forward light-scattering techniques for the size analysis of particles. In this method a measurement probe can be used

(9) Jillavenkatesa, A.; Dapkunas, S. J.; Lum, L. H. *Particle Size Characterisation: Practice Guide*; National Institute of Standards and Technology: Washington DC, 2001, Special Publication 960-1.

(10) *MasterSizer Operators Manual*Malvern Instruments Ltd., MAN 0247.

(11) Ma, Z.; Merkus, H. G.; van der Veen, H. G.; Wong, M.; Scarlett, B. *Part. Part. Syst. Charact.* **2001**, *18*, 243.

Table 1. **Size and shape parameters within the image analysis system together with their associated definitions**

parameter (name)	definition	units or range	additional information
area	visually projected area of the particle	pixels or μm	−
major axis	passes through the centre of mass of the object at an orientation corresponding to the minimum rotational energy of the shape	angle (deg)	Figure 4a
minor axis	passes through the centre of mass at right angles to the major axis	angle (deg)	Figure 4a
length	longest of all possible lines between two points on the perimeter projected on the major axis	μm	Figure 4b
width	longest of all possible lines between two points on the perimeter projected on the minor axis	μm	−
aspect ratio	width/length	between 0 and 1	needle shapes $\approx$ 0
elongation	1-aspect ratio	between 0 and 1	needle shapes $\approx$ 1
perimeter	total length of the boundary pixels	pixels	Figure 4c
CE (circle equivalent) diameter	diameter of a circle which has the same area as the 2D image of the particle	μm	Figure 4d
circularity (**H**igh **S**ensitivity circularity)	$2 \times \sqrt{\pi} \times$ (area/perimeter)	between 0 and 1	
convexity	parameter that measures the roughness of the particle		smooth surface = 1

Table 2. **Premeasurement settings within Morphologi prior to analysis of the images**

setting (name)	definition/explanation	chosen value/range
threshold	Aim is to correctly identify the particle edges; this is the point where a light grey "halo" starts to appear around the particles.	default: 105; for present study: between 169 and 171.
analysis ID	ID given by the software	software default
trash size	The size of the particles in pixels and any particle below this value is discarded from the analysis; used to reject small dirt particles as "noise", and the given value is chosen on the basis of the size of an average particle.	4
segmentation method	algorithm used to separate touching particles	see section 3.4 for explanation
fill holes	turned on if the area within a particle shape (e.g. a doughnut-shaped particle) is to be taken into account	ON

for online measurements within practical processing systems. The principle of backward light scattering is the basis adopted for the focussed beam reflectance measurement (FBRM),[12] and in this method a rotating beam of laser light is focussed on the edge of a particle in a suspension which is then reflected or scattered back when the beam hits the opposite edge of the particle. The scattered beam is collected by the probe, and from the time interval and the velocity of the beam, the particle's chord length and scattered intensity related to particle size and concentration can be derived. Chord length, which is not directly related to particle size distribution,[13] is the straight line between any two points on the edge of the particle. This method has an advantage of assessing the particle size distributions within the size range 0.8−1000 μm and can be applied in principle even in concentrated slurries in contrast to the transmission laser light scattering method.[14] Using the commercial Lasentec FBRM probe,[15] it is not straightforward to get the size of the crystals

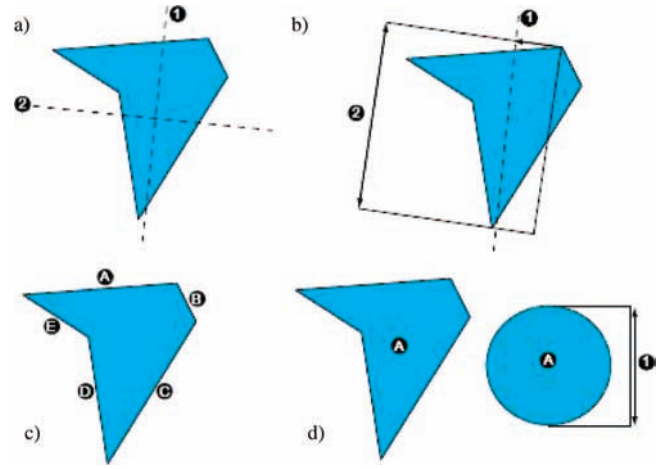

Figure 4. **Schematic representation illustrating the definitions of some of the shape parameters used in Morphologi software: (a) major axis (1) and minor axis (2); (b) length of the particle (2) i.e. longest line when projected on the major axis (1); (c) particle perimeter, i.e. A+B+C+D+E; (d) CE diameter; A denotes the actual particle which has an equivalent area of the circle shown whose diameter is given as 1.**

(12) http://us.mt.com.
(13) Hukkanen, E. J.; Braatz, R. D. *Sensors Actuators B* **2003**, *96*, 451.
(14) Barrett, P.; Glennon, B. *Trans. Inst. Chem. Eng.* **2002**, *80*, 799.
(15) http://us.mt.com/mt/.

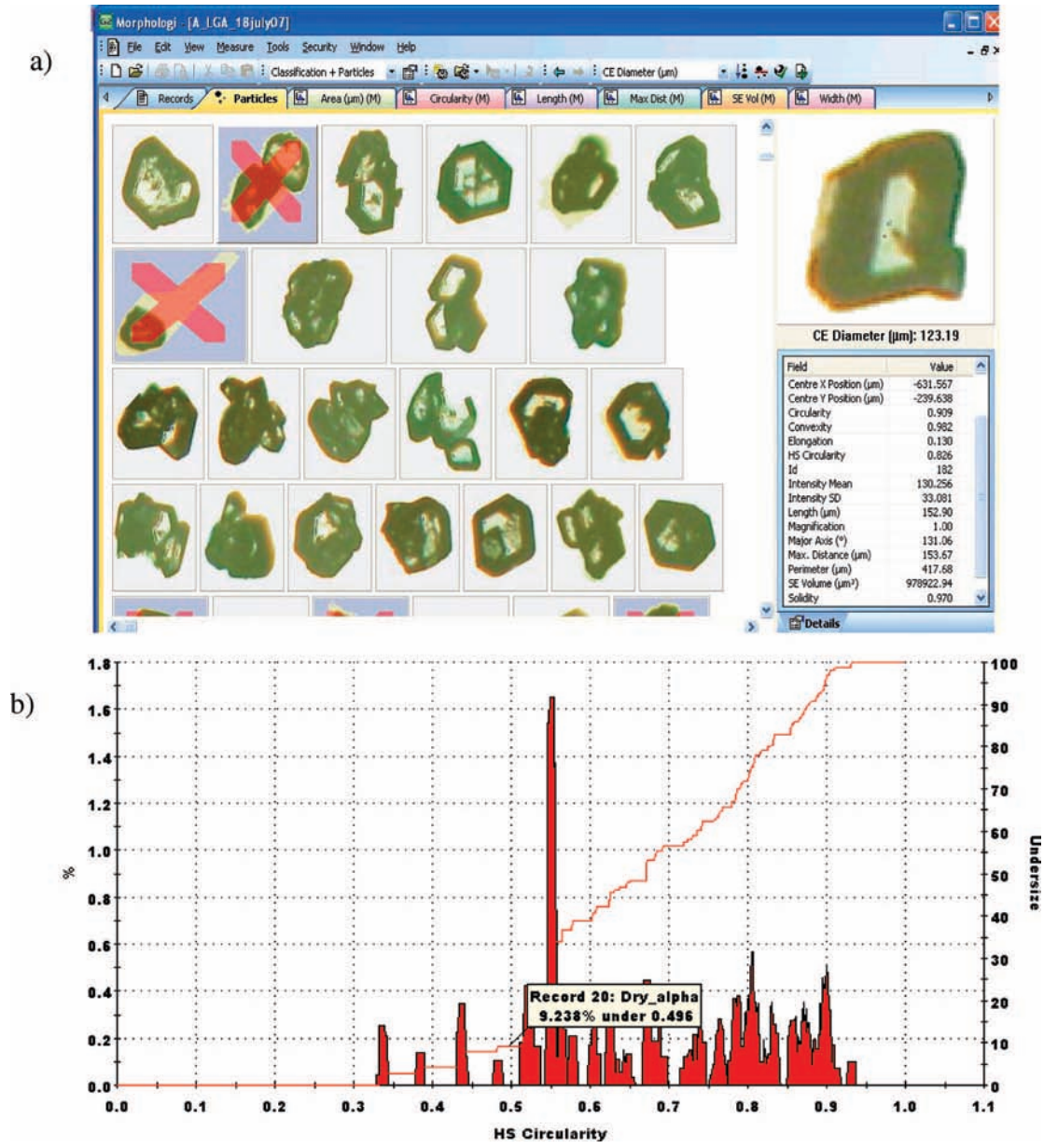

Figure 5. **Analysis of dry α-L-GA crystals using the Morphologi image analysis software; (a) screen shot of window showing particles displayed after segmentation and filtering. (b) Distribution of HS circularity after filtering. (The percentage of particle number is denoted on the primary *y*-axis, and the cumulative distribution of the shape factor is on the secondary *y*-axis. The red line denotes the undersize distribution, and any point on this line gives the percentage of particles below that particular value of HS circularity. An example is shown in the yellow box.)**

with different orientations directly from the chord length distribution, particularly for high aspect ratio particles, as there are some problems in the correlation between the particle size and the chord length[16,17] which can also limit the applications of this technique. When comparing with other established methods, this technique yields wider distributions for chord length measurements compared to the CSD, thus resulting in an underestimation of the particle size. A notable problem comes from the characterisation of nonspherical particles prepared during the crystallization of organic materials (typically needles and plates) where each particle, depending upon its mutual orientation with respect to the FBRM beam, can yield a chord length distribution. When measuring at high particle concentrations, the effectiveness of the technique for both size and concentration assessments can also be limited.

Ultrasonic attenuation spectroscopy, based on the attenuation of ultrasonic waves transmitted through a solid−liquid suspension,[18] is an emerging technique for particle size characterisation. The ultrasonic attenuation spectrum depends on the solid concentration and the size of the particles. Generally, the crystal size distribution can be derived from the attenuation spectrum[19,20] The strengths of this technique is that it provides rather accurate measurements of both the particle concentration and

(16) Ruf, A.; Worlitschek, J.; Mazzotti, M. *Part. Part. Syst. Charact.* **2000**, *17*, 167.
(17) Tadayyon, A.; Rohani, S. *Part. Part. Syst. Charact.* **1998**, *15*, 127.
(18) Richter, A.; Babic, F.; Ripperger, S. *J. Acoust. Soc. Am.* **2005**, *118*, 1394.
(19) Epstein, P. S.; Carhert, R. R. *J. Acoust. Soc. Am.* **1953**, *25*, 553.
(20) Allegra, J. R.; Hawley, S. A. *J. Acoust. Soc. Am.* **1971**, *51*, 1545.

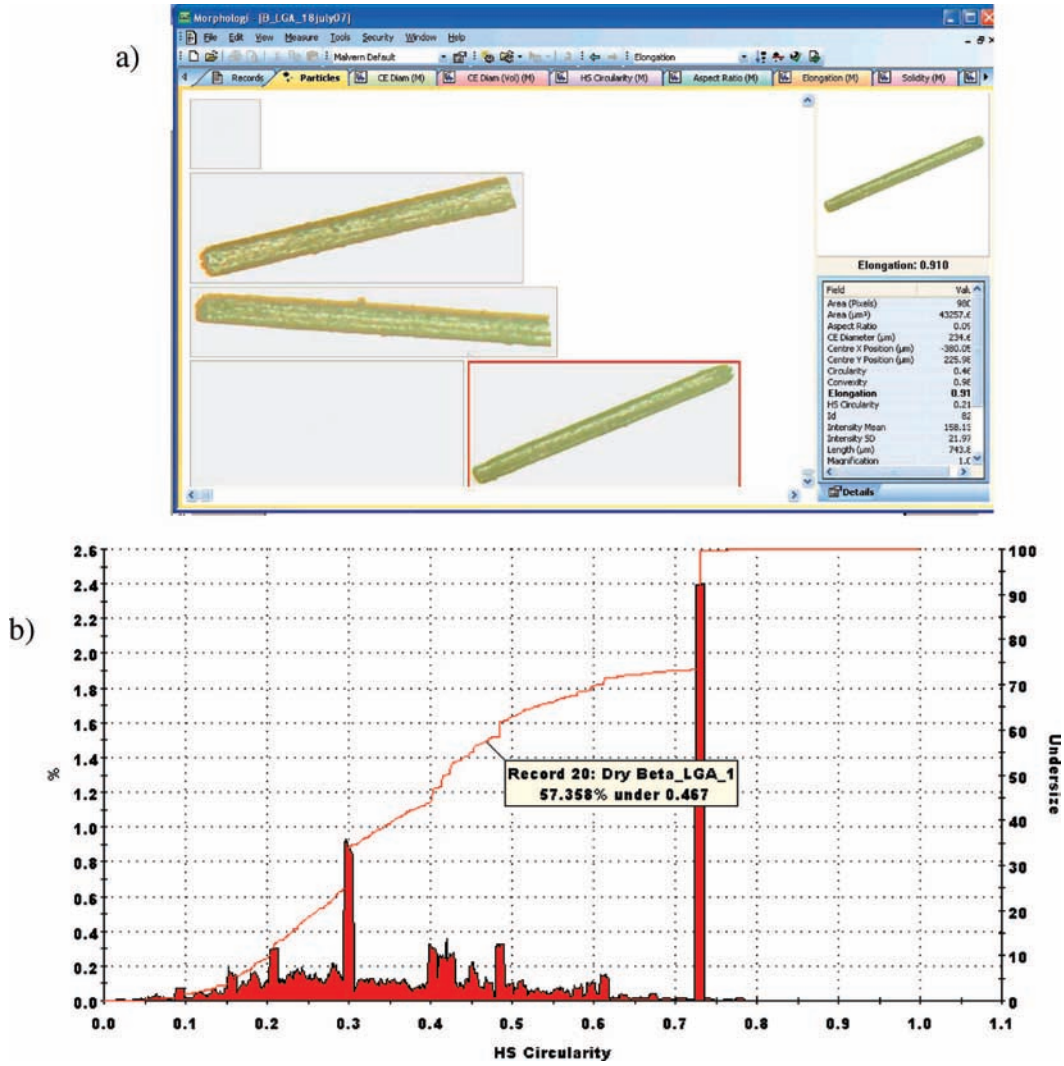

Figure 6. **Analysis of about 1500 particles of dry β-L-GA crystals using Morphologi image analysis software. Particles with an elongation of less than 0.45 were filtered out since these particles are not characterised by the needlelike shape of β crystals: (a) screen shot of some of the particles after sorting; (b) distribution of HS circularity showing more than 50% of particles have circularity below 0.46; the primary *x*-axis shows the percentage of particles with a particular value of the shape factor, and the secondary *y*-axis represents the cumulative distribution of particles for the respective shape factors.**

its CSD, albeit in common with laser light scattering the technique has its limitations for particles with high anisotropic shape such as needles.[21] The technique has been applied to crystallization monitoring via the use of a flow-through cell and particle growth rate data obtained.[22] Flow-through process analytical techniques are highly valuable for in-process analysis and control chemical processes. It is also worth noting that these techniques are applied to continuous rather than batch processing.

Microscopy-based techniques for particle size measurements can be powerful tools,[23] and generally in these techniques, the calculated size is expressed as a volume equivalent diameter i.e., a sphere that has the same projected area as the diameter of the image of the particle. The other measurements, such as area, mass, or volume, can be derived from the diameter. This technique has the advantage that shape of particle can be determined in addition to size. Instruments using microscopy-based techniques typically are the optical microscope, scanning electron microscope (SEM), and transmission electron microscope (TEM) with the suitability of the instrument being based on the size of the particles needing to be analysed. Optical microscopes are affordable, easy to operate, require simple sample preparation when compared to requirements for SEM or TEM, and can be used where the average particle size is ≥ 1 μm (particles from about 150 to 0.8 μm).[6] However, the depth of the focal field of optical microscopes may limit the accuracy in samples with wide particle size distributions; the accuracy of volume measurements is limited due to the preferential orientation of the particles; and the overall performance of these microscopes is limited by the wavelength of visible light. Transmission electron microscopy is useful when the particles are in the size range 0.01−10 μm and the disadvantages of using this technique are sample preparation, skill to operate the instrument, and due to the fact that only a few particles are

(21) Mougin, P.; Wilkinson, D.; Roberts, K. J. *Cryst. Growth Des.* **2002**, *2*, 227.
(22) Mougin, P.; Thomas, A.; Wilkinson, D.; White, G.; Roberts, K. J.; Herrmann, N.; Jack, R.; Tweedie, R. *AIChE J.* **2003**, *49*, 373.
(23) Jillavenkatesa, A.; Dapkunas, S. J.; Lum, L. H. *Particle Size Characterization: Practice Guide*; National Institute of Standards and Technology: Washington DC, 2001, Special Publication 960-1.

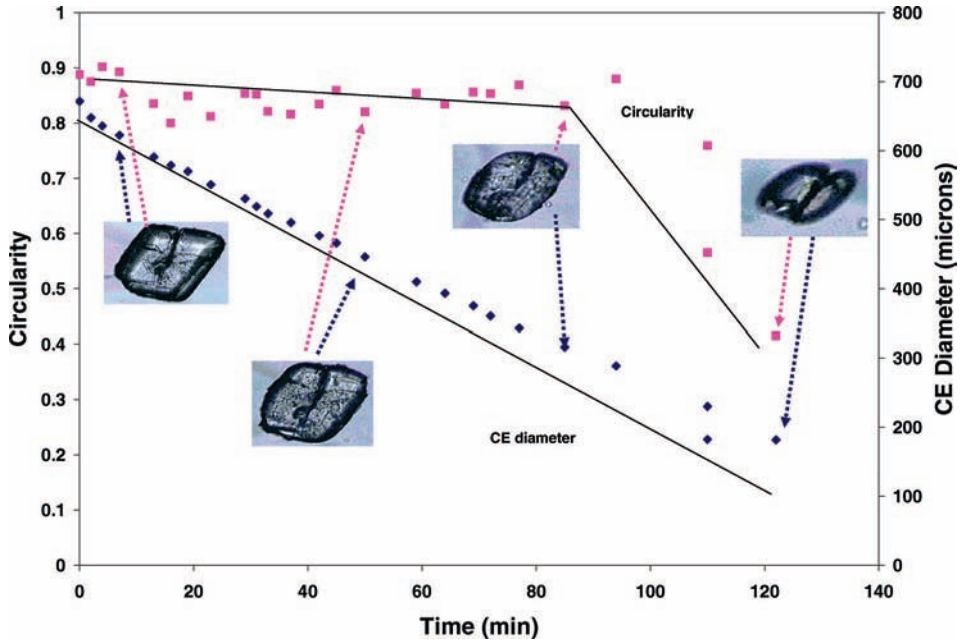

Figure 7. **Particle shape factors derived through image analysis from the hot-stage images of α-L-GA in saturated solution at 42.5 °C showing the dissolution with time within the dissolution process. The variation of CE diameter and circularity with time together with associated trend lines show that the particle is losing its circularity in addition to some roughening around the edges (between 90 and 100 min) and a linear decrease in the CE diameter. Four of the hot-stage images are overlaid on the plots to give an idea of how the crystals follow a largely facetted mechanism albeit with some rounding of the particle edges.**

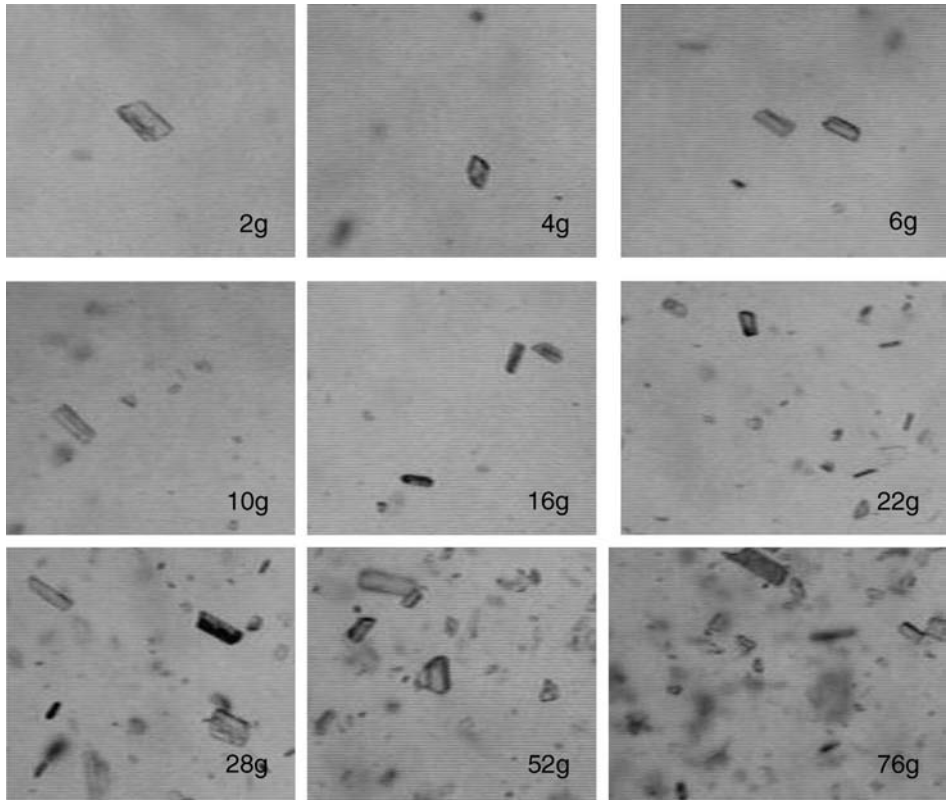

Figure 8. **ISPV data showing images as extracted from the video clips recorded during the slurry experiments where *β*-L-GA crystals were added to the slurry at intervals of about 10 min. The corresponding solid concentrations are marked in each image.**

examined, there may be a sampling error. Scanning electron microscopy also provides higher magnification and depth of focus compared to optical microscopy and is suitable for particles of sizes 0.1−1000 μm.

Most of the techniques used to determine CSD, including those discussed above, do not include the routine assessment of crystal shape determination which affects the accurate characterisation of particle size. Morphological molecular

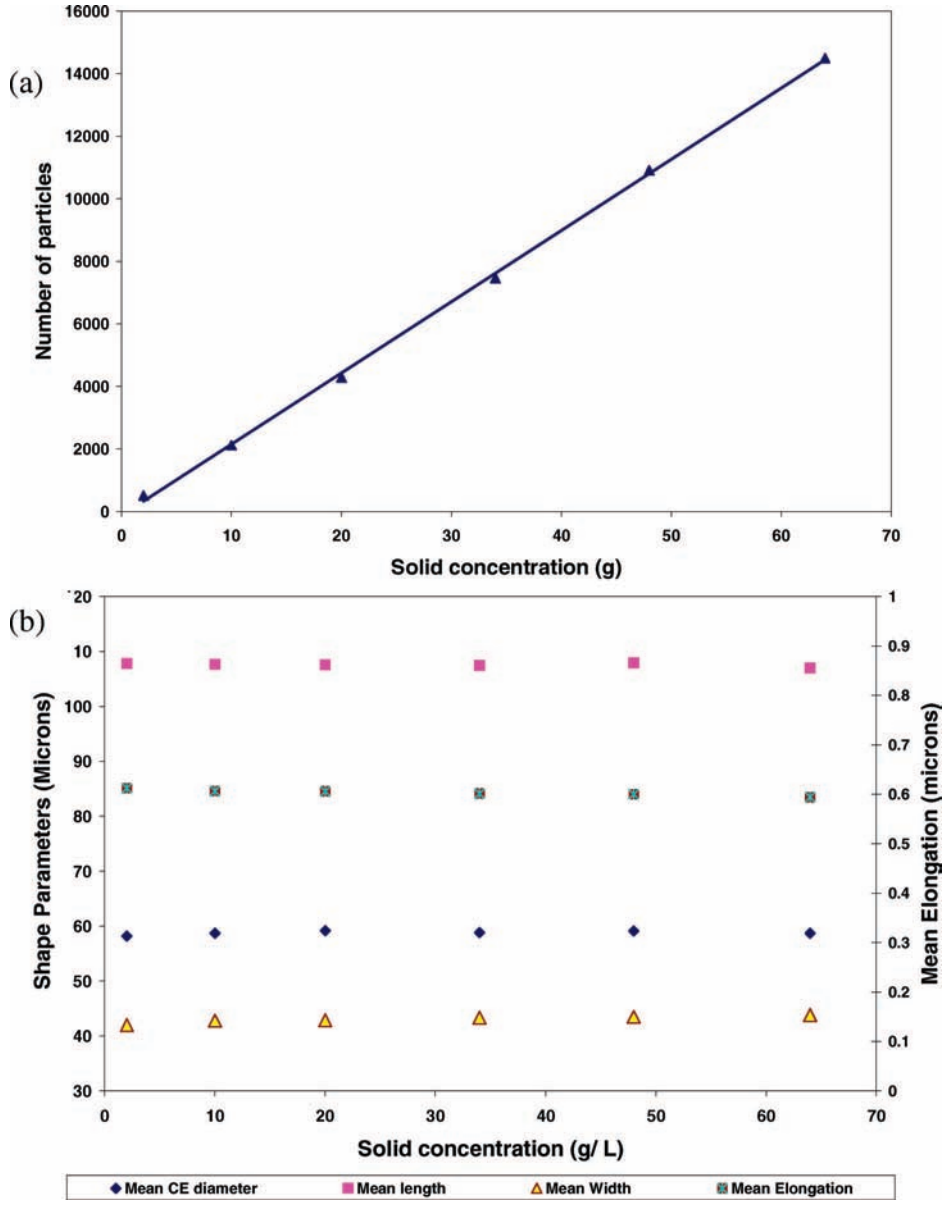

Figure 9. **Image analysis of the first slurry experiment, showing (a) a linear increase in particle number with solid concentration and (b) calculated shape factors (μm) vs solid concentration (g/L), revealing no significant variation during the experiment.**

modelling plays an important role in predicting the crystal shape which can be used to identify in situ crystal forms.[24] Microscopy and prediction methods have led to the successful characterisation of the morphology of several organic systems.[25–27]

A number of PAT instrumentation systems for evaluating crystal shape and size based on Digital Video Microscopy techniques. The particle view and measurement (PVM) system by Mettler Toledo is an in-process microscope.[28] The PVM has a slim probe which is suitable for small-scale vessels and has a high resolution video microscope imaging pictures of the crystals gives quantitative information on size and shape of particles of size ranging between 2 and 1000 μm without any need for sample preparation or sample extraction. PVM can be used in high concentration and it is capable of imaging solids in liquids, solids in gases, and liquid dispersions in liquids. PVM has been used as a complementary method to FBRM measurements for combined particle shape and size analysis.[29,30] Other PAT imaging systems include Process Image Analyser[31] (PIA) by MessTechnik Schwartz GmbH, Sysmex FPIA-3000,[32] PharmaVision System (PVS)[33] and Morphologi G3 by Malvern Instruments. An online digital video imaging instrument developed by GlaxoSmithKline,[34,35] has been used to carry out measurements of particle size and shape. This system, which

(24) Li, R. F.; Thomson, G. B.; White, G.; Calderon De Anda, J.; Wang, X. Z.; Roberts, K. J. *AIChE J.* **2006**, *52*, 2297.
(25) Docherty, R.; Roberts, K. J. *J. Cryst. Growth* **1988**, *88*, 159.
(26) Clydesdale, G.; Hammond, R. B.; Roberts, K. J. *J. Phys. Chem. B* **2003**, *107*, 4826.
(27) Clydesdale, G.; Roberts, K. J.; Walker, E. M. The Crystal Habit of Molecular Materials: A Structural Perspective. In *Theoretical Aspects and Computer Modelling*; Gavezzotti, A., Ed.;John Wiley & Sons Ltd.: Chichester, 1997.
(28) http://us.mt.com.
(29) Barrett, P.; Glennon, B. *Trans. Inst. Chem. Eng.* **2002**, *80*, 799.
(30) Scholl, J.; Bonalumi, D.; Vicum, L.; Mazzotti, M.; Muller, M. *Cryst. Growth Des.* **2006**, *6*, 881.
(31) http://www.mts-duesseldorf.de.
(32) *Sysmex FPIA-3000 brochure*; Malvern Instruments Ltd.
(33) *PVS-830 brochure*; Malvern Instruments Ltd.

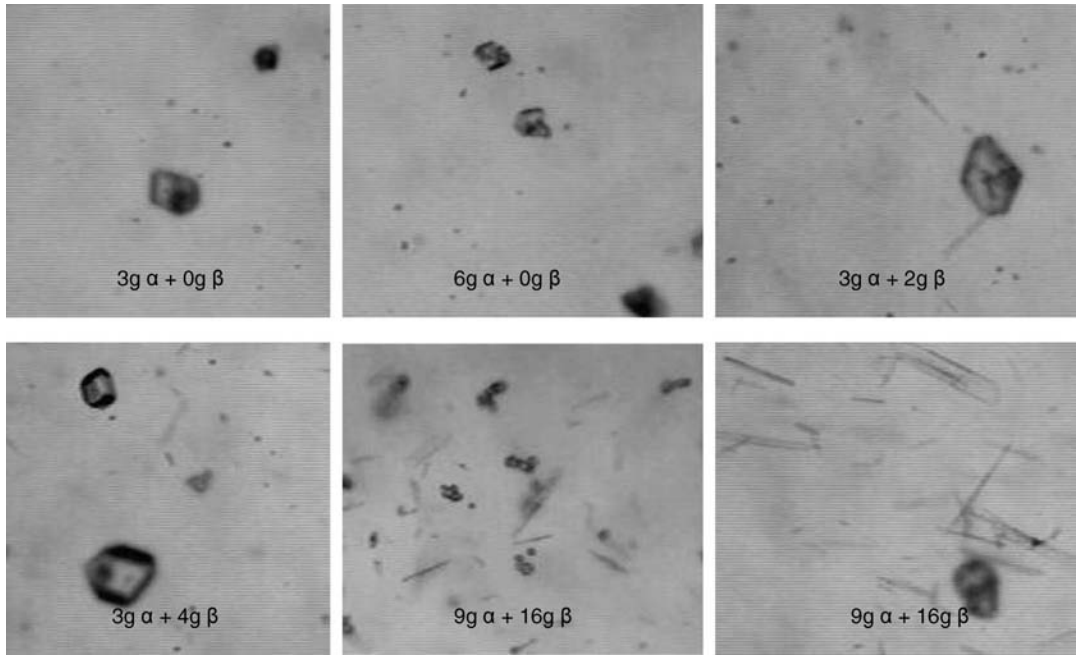

Figure 10. **Section of six sample images extracted from the video sequence for the second of the experiments with the crystal/solution slurries.**

is not commercialised, is noninvasive as it is outside the vessel and it can record real-time images. The system has been integrated with sophisticated image analysis techniques[36] for improved image definition and has been combined with morphological prediction for both phase identification in polymorphic conversion studies and growth rate determination.[37] In-Situ Particle Viewer is a new type of imaging probe developed by Perdix Technologies B.V., Netherlands,[38] which provides real-time information on particle parameters such as size, geometry and surface properties. The assessment of this system forms the basis of this paper. Its mode of operation is described in section 3.3. The in situ studies using the ISPV system are integrated with detailed characterisation of the particle shape of the two LGA polymorphic forms together with hot-stage microscopy studies to characterise the basic growth/dissolution and phase transformation behaviour prior to studies at 20-L scale size. In this, the aim has been to assess the utility of this probe system for practical process-scale studies of crystallization processes and to assess the strengths and limitations of this available technology.

3. Materials and Methods

3.1. Materials. The crystallization characteristics[39,40] and its phase transformation properties[41,42] of L-GA are well-known. L-GA is a zwitterionic amino acid, and it has two polymorphic forms, viz. the metastable α- and stable β-forms. Both forms can be crystallised from aqueous solutions at varying cooling rates (slow cooling yields the β-form, and fast cooling results in the α-form). Dry crystals of the metastable α-phase are highly stable but slurried in a saturated solution of LGA, a solvent-mediated polymorphic transformation occurs involving dissolution of the α-form and regrowth of the stable β-form. Panels a and b of Figure 1 show the microscopic images of dry powders of the α- and β-forms of L-GA, revealing the prismatic shape of α-L-GA and the needlelike shape of β-L-GA with the differences in crystal morphology reflecting differences in the molecular conformation and packing anisotropy of the respective forms. L-GA in its β-form was purchased from VWR international, and solutions were prepared using distilled water.

3.2. LGA Precharacterisation Using Optical and Hot-Stage Microscopy. A standard reflected light Olympus IMT-2 microscope (objective lens magnification 4×) with a CCD camera (JVC model KY-F1030) and a KY-LINK image acquiring package was used for microscopic investigations of dry L-GA crystals. These dry powder experiments were carried out with pregrown α-L-GA and β-L-GA crystals.

Hot-stage optical microscopy was carried out using a Leica-DMLM microscope fitted with a Pulnix TMC-312 digital camera (image size 0.85 mm × 0.62 mm) and a Linkam LTS-350 hot-stage[43] having a working temperature range −196 to 350 °C and stability <0.1 °C. The hot-stage has a sample area 40 mm × 40 mm, and the sample is mounted on a standard microscope slide (76 mm × 26 mm) in direct contact with the polished heating element which can be manipulated 15 mm in *X* and *Y* directions. A platinum resistor, embedded close to the surface of the sample, monitors the sample temperature. A small

(34) Calderon De Anda, J.; Wang, X. Z.; Lai, X.; Roberts, K. J. *J. Process Control* **2005**, *15*, 785.
(35) Calderon De Anda, J.; Wang, X. Z.; Lai, X.; Roberts, K. J.; Jennings, K. H.; Wilkinson, M. J.; Watson, D.; Roberts, D. *AIChE J.* **2005**, *51*, 1406.
(36) Calderon De Anda, J.; Wang, X. Z.; Roberts, K. J. *Chem. Eng. Sci.* **2005**, *60*, 1053.
(37) Calderon De Anda, J.; Wang, X. Z.; Roberts, K. J. *Chem. Eng. Res. Des.* **2007**, *85*, 921.
(38) http://www.perdix.nl/frames.html.
(39) Kitamura, M. *J. Cryst. Growth* **1989**, *96*, 541.
(40) Shan, G.; Igarashi, K.; Noda, H.; Ooshima, H. *Chem. Eng. J.* **2002**, *85*, 169.
(41) Ferrari, E.; Davey, R. J. *Cryst. Growth Des.* **2004**, *4*, 1061.
(42) Ono, T.; ter Horst, J. H.; Jansens, P. J. *Cryst. Growth Des.* **2004**, *4*, 465.
(43) http://www.linkam.co.uk/.

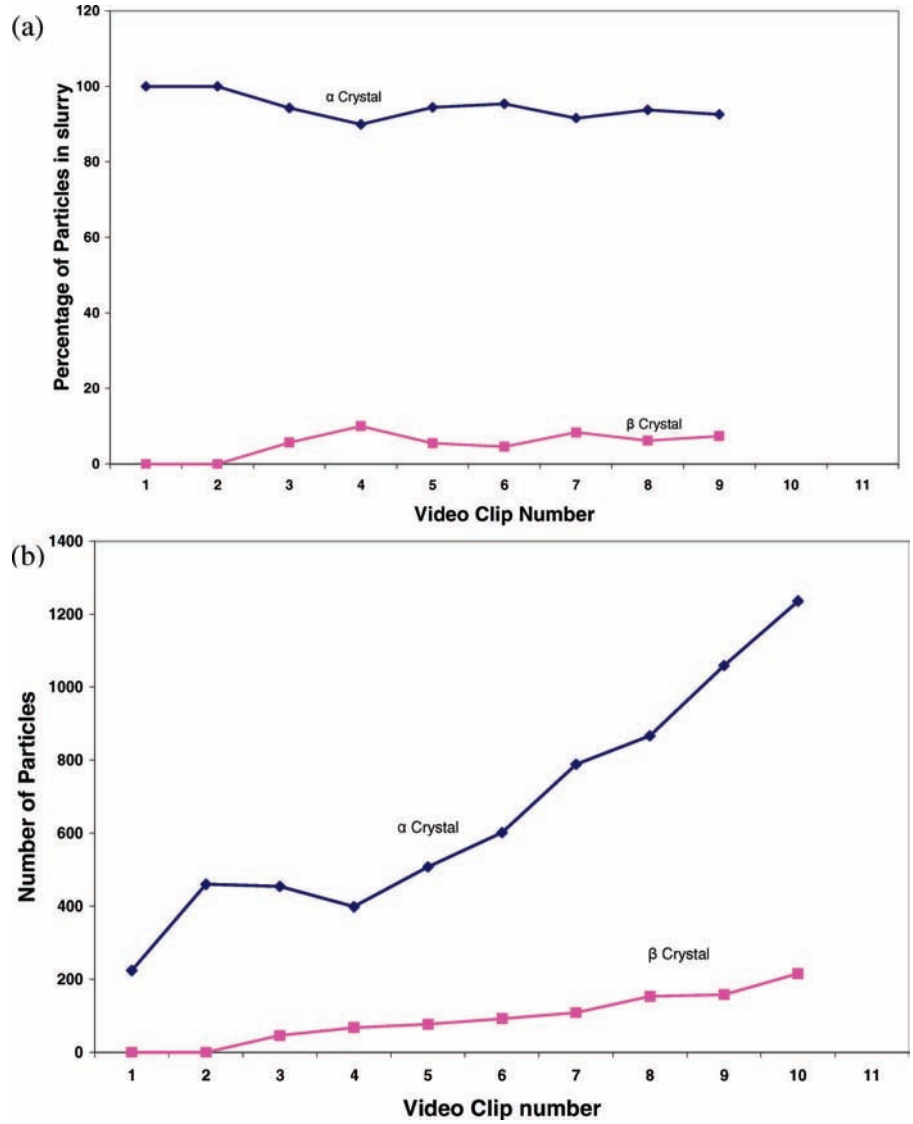

Figure 11. **Image analysis of the second slurry experiment: (a) percentage of α and *β* crystals in the slurries; (b) number of α and *β* crystals in the slurries.**

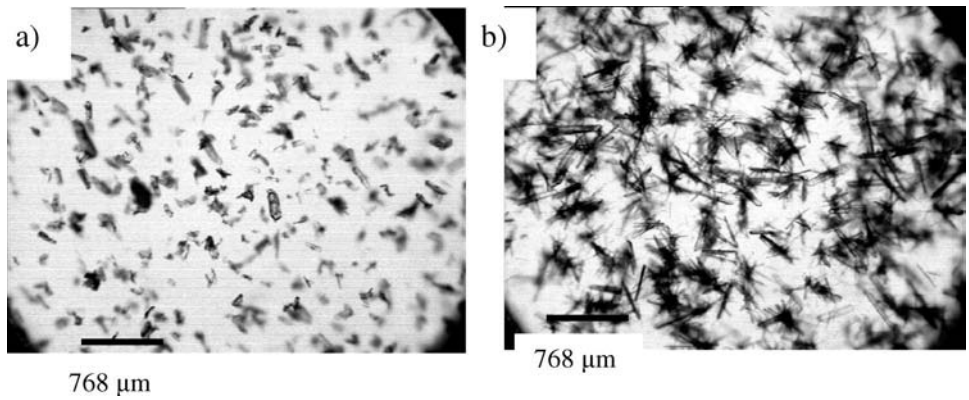

Figure 12. **ISPV images recorded during the seeded crystallization of *β*-form L-GA: (a) seed crystals which were added to the solution at 65 °C; (b) growing *β*-L-GA crystals during the experiment at about 35 °C, before the encrustation effect began.**

light aperture, size 2.5 mm ∅, reduces the temperature gradient across the sample. The minimum working distance of the objective lens is 6 mm. For the solution studies, a small quartz cell of ∼1.5 cm in diameter and ∼2 mm height covered with a glass coverslip (to maintain the sample temperature) was used. Transmitted light together with a 1.25 condenser and (5×) objective lens were found to provide a good contrast between background and the particles. The purpose of the hot-stage experiments was to monitor crystallization and polymorphic transformation of organic systems with the hot-stage microscope and use these data for further image analysis. One of the experiments whose results are reported in this paper is detailed

here. The polymorphic transformation experiment involved the observation of a seed crystal of α-L-GA in a saturated solution at 42.5 °C over a period of time. The saturated solution was prepared with 0.7937 g in 50 mL of distilled water. Complete dissolution was achieved using a hot plate and a magnetic stirrer.

3.3. Studies Using an ISPV System at 20-L Scale Size. The ISPV system probe as shown in Figure 2a is 1.8 m long and is suitable for use in large processing vessels and has a probe sensor head (Figure 2b) comprising a built-in CCD video camera for acquiring real-time images. The probe is connected to a control box that has an appropriate stroboscopic light source. The probe is designed for temperatures up to 150 °C and to minimize flow distortions and resist high pressures. A water jacket is provided to cool the sensor head so that in principle the probe's temperature range can be extended. Figure 3 shows the experimental setup comprising the 20-L reactor equipped with the ISPV probe. The ISPV camera gives direct transmission imaging and has a fixed focus length with the positions of both camera and the illuminating light strobe being fixed with a field of view of about 8 mm × 6 mm, a resolution of 40 μm, and 768 pixels × 576 pixels. The strobe provides backlight illumination giving excellent contrast to the images and accurate quantitative information. The applications of the Perdix probe include monitoring the changes during crystallization processes and quality control processes.

A HEL Autolab reactor system, used for the experiments, comprises a 20-L jacketed glass reactor (Figure 3), a Huber thermostatted bath, a data interface board (A/D), and a PC running WindowsXP with WinISO process control software (HEL Ltd.). The reactor has a diameter of 0.3 m and was used with a 1:1 hydrodynamic ratio of width to height). Tthe stirring was provided with the use of a retreat curve impeller (RCI) of diameter 0.2 m, rotating at a constant speed of 100 rpm. The angle of the ISPV probe was approximately 10−15°, and the tip of the probe was half-immersed vertically from the bottom (not far from the impeller so that the mixing is not affected) in the vessel content volume for all of the experiments.

The temperature and turbidity (to detect crystallization onset) were measured using a platinum resistance thermocouple (PT100) and turbidimetric fiber-optic probe. A number of proof of concept experiments (slurry and crystallization experiments) were carried out with the ISPV system using the 20-L Autolab reactor system. The angle of the ISPV probe was approximately 10−15°, and the tip of the probe was half-immersed vertically from the bottom (not far from the impeller so that the mixing is not affected) in the vessel content volume for all of the experiments.

3.3.1. Slurry Experiments. Three slurry experiments were carried out. In the first two experiments, the slurry was prepared and kept at 20 °C, and the particles (α-L-GA particles in the first and both α-L-GA and β-L-GA in the second) were added approximately every 10 min, and the video was recorded. The third slurry experiment was the polymorphic transformation experiment for which the slurry was prepared at 20 °C and was heated to 58 °C. For these experiments, the ISPV probe temperature was 30 °C. The probe temperature was different from the solution temperature for these experiments because we used the optimum temperature for probe which is 30° C (for optimal performance of the camera as suggested by the manufacturer), and the stirrer speed was 100 rpm.

3.3.2. Crystallisation Experiments. Spontaneous crystallization experiments to crystallise both α- and β-phase particles including the assessment of changes in probe temperature were carried out. In the first of the two α-LGA crystallization experiments, a saturated solution was prepared at 53 °C (24 g/L), and the probe temperature was set to 40 °C; for the second experiment, saturated solution was prepared at 70 °C (44.4 g/L), and the probe temperature was set to 45 °C which was then followed by cooling at rates of 0.5 °C/min. For the β-crystallization experiment, a saturated solution was prepared at 70 °C (44.4 g/L) and then cooled at the rate of 0.1 °C/min. For the seeded crystallization experiments to crystallise β-phase particles, a saturated solution of L-GA (44.4 g/L) was prepared at 70 °C and was heated to 80 °C for complete solid dissolution, and the crystallization process was aided by 10 wt % of seed β-L-GA crystals at 65 °C before cooling it to 10 °C at a rate of 0.25 °C/min.

3.4. Image Analysis Techniques. Particle size and shape analysis of all the images have been carried out by Morphologi software (www.malvern.co.uk). A number of shape parameters of 3D particles are derived from their 2D images, and from these parameters, the statistical data such as mean, median, mode, standard deviation, etc. can be calculated. The parameters used in this software are summarised in Table 1. Prior to analysing any image, premeasurement settings are entered which include sample details, threshold, and analysis settings. The definitions of these settings and the chosen values during the analysis of the images are presented in Table 2.

There is only one segmentation method available in the current version (watershed) which is not suitable for needlelike particles. The image segmentation algorithm used in Morphologi is specifically designed to operate with "round", separate but touching particles and is not suitable for needlelike particles. In addition, images from the probe have a nonuniform background intensity, and simple thresholding does not give good particle segmentation over the time frame. For this reason, prior to the analysis of the data that involved β particles an alternative algorithm was used to preprocess.

4. Results and Discussion

4.1. LGA Precharacterisation Using Optical and Hot-Stage Microscopy Studies. The image analysis of these initial optical microscopy experiments has provided a basis for the analysis of the images recorded using ISPV probe during the slurry experiments with L-GA crystals.

4.1.1. Studies of the Dry Particles. Analysis of optical microscope images of dry α- and β-L-GA crystals (Figure 1 a and b, respectively) was carried out by eliminating all particles with circle equivalent (CE) diameters <75 μm and elongation <0.3 in order to classify prism-shaped α-L-GA, and particles with an aspect ratio >0.55 (elongation <0.45) were eliminated to classify the needle-shaped β particles. The filtering parameters are chosen from the values of an average particle with a characteristic shape. In addition, as the resolution was not high enough for some β-L-GA particles to separate from the

background, those particles were eliminated from counting. Some of the α particles after filtering are presented in Figure 4 and Figure 5a. From the shape factors, HS circularity after filtering (Figure 5b), it is clear that these particles are highly circular (average circularity is 0.86 where 1 is for a perfect circle), and the average aspect ratio of these particles is 1. From examples from a total of 1500 particles, the classified β particles are shown in Figure 6a. Figure 6c presents the distributions of elongation and HS circularity, revealing that a large fraction of the particles are not circular but elongated with an average HS circularity at 0.42, in contrast to the α particles which have an average HS circularity of 0.86. The technique confirms the obvious advantage in that it provides a methodology for particle size/shape analysis which can be used in conjunction with appropriate in-process sensors. With a Pentium 4 processor and 1 GB of RAM, the CPU times taken for processing the images range from 30 min up to 3 h, depending on the number of images processed and the number of particles on each image.

4.1.2. Hot-Stage Studies. Initial hot-stage experiments combined with image analysis provided some interesting observations of the dissolution and growth of the seed crystals in solution and also polymorphic transformation. The analysis of the hot-stage images obtained during the polymorphic transformation experiment along with some images overlaid on these plots is shown in Figure 7. These plots and the images show clearly the dissolution process with time, and the crystal is completely dissolved after about 130 min. The rate at which the CE diameter decreases is another indication of the rapid dissolution of the particle. The particle remained circular for most of these observations, and it loses the circularity rapidly after about 90 min. In addition to the seed crystal, at least one needlelike particle is seen in the images which could be a β-L-GA crystal nucleating within the solution.

4.2. Studies Using the ISPV System. *4.2.1. Slurry Experiments.* The images captured at varying solid concentrations during the first of the two slurry experiments are given in Figure 8. The recording of each video consisted of 300 frames, with the last 100 frames being used to derive the shape and size information using image analysis. Parts a and b of Figure 9 report the resultant analysis with the first plot showing a linear increase in the particle number with solid concentration and the second plot providing the shape-dependent data: CE mean diameter, mean length, and mean width of particles with solid concentration, with the mean values of the shape parameters not showing much variation with the increase in solid particle concentration.

In the second slurry experiment both α and β crystals of L-GA were added to the slurry. A sample of six images from the frames set for different solid concentrations is shown in Figure 10 Different quantities of the two polymorphic forms were simple added to assess the camera's performance. Pleasingly, the image analysis picks out the two characteristic shapes, even though it is very hard to distinguish the needlelike morphologies. This is clear from Figures 10, and 11a and b which show the fraction of α and β crystals, and the total number of each type of particle, respectively. It should be noted that since β particles have a grey intensity that is very close to the intensity of the background, the image segmentation method embedded into the software could not extract many of these β crystals from these raw images.

In the third slurry experiment the objective was to assess whether the α-to-β polymorphic transformation could be followed, i.e. through monitoring in the respective changing concentrations. However, the quality of these images was not found to be suitable for analysis primarily due to magnification issues; i.e. the small size of β crystals ($\sim$10 μm) and the formation of a high number of crystals within the field of view made it difficult to reliably differentiate the β-form crystals from those of the α-form.

4.2.2. Crystallization and Polymorphic Transformation Experiments. Nonseeding crystallization experiments of α- and β-forms of L-GA were dominated by encrustation effects due to direct crystallization on the measurement optics, and hence the data were not suitable for detailed image analysis. The onset of mass crystallization, which is marked by a sudden change in solution turbidity, was immediately followed by encrustation; within an hour the entire surface of the lens was covered with crystals. During this experiment, the stirrer speed was increased from 100 to 160 rpm in an unsuccessful attempt to increase the rate of flow through the gap between the camera lens and the camera strobe and reduce the encrustation of crystals. The camera performance is optimal at about 30 °C, and it is cooled with an external bath set up at 30 °C during crystallization experiments. The low temperature of the camera probe at the onset of crystallization unfortunately favours nucleation on its surface as the solution in contact with this is more supersaturated compared to the solution elsewhere in the reactor.

The major factors that are responsible for material encrustation are the chemistry of the camera surface and the solute molecules. In addition, the temperature difference between the probe and solution has an influence on encrustation. Hence, a crystallization experiment with a higher probe temperature was carried out to observe if the encrustation activity was reduced or if it was overcome completely. There were only a few crystals stuck to the surface of the camera in contrast to the previous experiments where the entire surface of the camera lens was covered by crystals.

Successful monitoring was achieved via controlled seeded crystallization experiments with the presence of seed crystals in the solution minimising the heterogeneous 2D nucleation by consuming the available supersaturated solution for the expense of the growth of seed crystals. Online images of the seed crystals and the growing crystals are shown in Figure 12. The seeds were added at about 223 min after the start of the experiment. Soon after this, video images were recorded. An analysis with a set of images which were recorded for a period of about 50 min towards the beginning of the cooling process (approximately 20 min after the addition of the seed crystals) was carried out with Figure 13 showing the correlation between the variation of the shape factors such as perimeter, width, and length and time. The increasing trend of these shape parameters, especially the mean perimeter of the crystals, clearly indicates the presence of crystal growth. As there were too many β-L-GA crystals during growth and as the encrustation effect became dominant towards the end of the experiment, it was not feasible to carry out a complete analysis. However, the presence of seed crystals

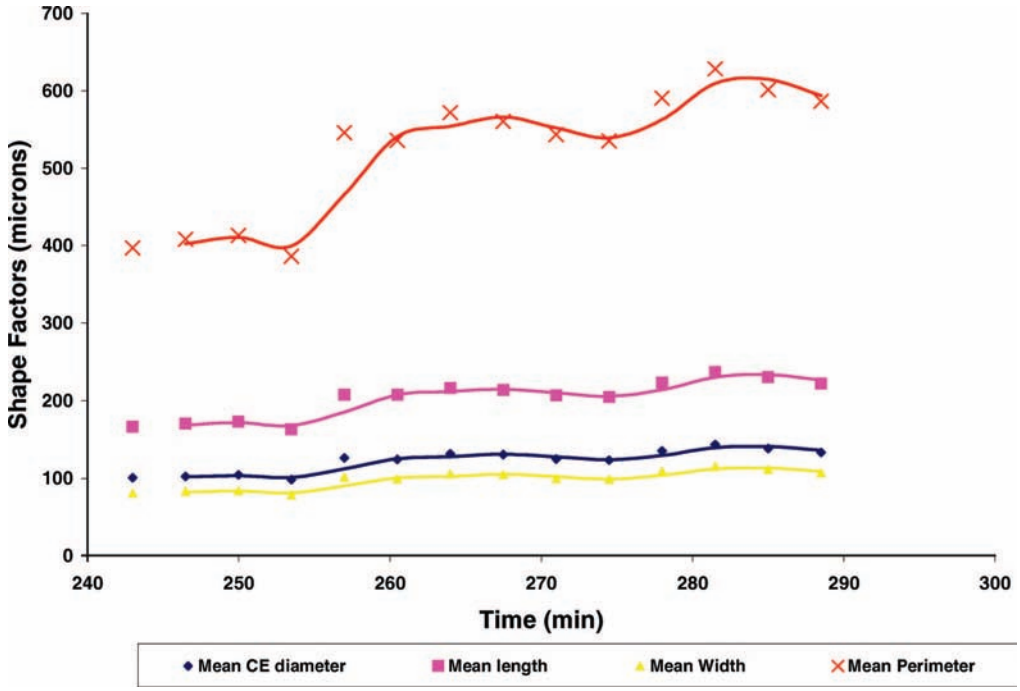

Figure 13. **Analysis of the images captured during seeded crystallization (after about 20 min since adding the seed crystals and at a temperature of 60 °C) of β-form L-GA showing the variation of the shape factors with time. Crystal growth has an effect on these shape factors that show an increasing variation with time; this increase is very prominent in the mean perimeter. The trend lines represent the moving average.**

in the solution minimised the homogeneous and heterogeneous 2D nucleation by consuming the available supersaturation at the expense of seed crystals growth.

5. Conclusions

This work has provided an insight into how the ISPV probe can facilitate real-time images for visually identifying key stages of crystallization processes such as onset, growth and polymorphic transformation of the crystals. In addition, detailed image analysis using the Morphologi software has provided some process information about crystal shape and size and its evolution during crystallization. The system confers clear advantage for using large-scale process reactors compared to other commercial systems.

The existing ISPV probe system has clear potential applications for monitoring and controlling the large-scale crystallization reactors due to its size and mechanical strength, whilst its transmission geometry confirms distinct advantages over existing back-reflection technology. However, further developments of ISPV probe for in situ crystallization studies are clearly needed to optimise its applications including provision of full range in-process analysis tools together with increasing spatial resolution, thus improving its ability to image small or needle-like crystals. In addition, potential exists regarding possible use with a polarized light source to improve crystal definition via extraction of the birefringence effects for organic speciality solid systems. The current probe also suffers, to a degree, from encrustation effects particularly for L-GA, and further work is needed to effect better thermal insulation for the probe to ascertain if this issue is a generic or system-specific probe.

Finally, options to exploit this system in an integrated approach including manufacturing with upstream process research and development clearly require a complementary smaller-scale system for routine high throughput and laboratory-scale work. Work on this aspect is currently in hand and will be reported in a future publication.

Acknowledgment

This work was funded by the Malvern/Leeds Intellisense Alliance in Integrated Process systems drawing down on previous research and experimental facilities developed through the Chemicals Behaving Badly II initiative (http://www.leeds.ac.uk/chemeng/CBB/cbb2.html), a collaborative EPSRC/DTI project involving ANSYS Europe Ltd., AstraZeneca, Bede Scientific Instruments Ltd., Malvern Instruments, Pfizer, BNFL, GlaxoSmithKline, HEL, Clairet Scientific and Syngenta.

Supporting Information Available

Analysis of dry α-L-GA crystals using the Morphologi image analysis software are shown in Figure SA1a−c which are HS circularity before filtering, aspect ratio of the particles before and after filtering, respectively. Figure SA2 shows the distribution of eleongation of β-L-GA crystals. Images obtained during the polymorphic transformation experiment within a hotstage are given in Figure SA3 clearly showing the dissolution of an α-L-GA crystal with time at a solution temperature of 42.5 °C with the crystal dissolved completely after about 130 min. Some of the images from the seeded crystallization experiments are presented in Figure SA4a,b. This experiment could not be continued below 41 °C due to the effect of moisture condensation. However, there were significant changes to the crystal faces (Figure SA4b). The analysis of the first set of images showing dissolution is given in Figure SA5a,b revealing the CE diameter and perimeter to decrease with decreasing

temperature. The quality of the images (Figure SA6) taken during one of the slurry experiments was not found to be suitable for analysis primarily due to magnification issues, i.e. the small size of β-crystals ($\sim$10 μm) and the formation of a high number of crystals within the field of view made it difficult to reliably differentiate the β-form crystals from those of the α-form. Nonseeding crystallization experiments of α- and β-forms of L-GA were dominated by encrustation effects (Figures SA7a−d) due to direct crystallization on the measurement optics; hence, the data were not suitable for detailed image analysis. This material is available free of charge via the Internet at http://pubs.acs.org.

Received for review January 18, 2008.

OP800011V